APPENDIX

Analytical methods

We determined $S^{6+}/\Sigma S$ ratios of lunar apatites, mesostasis glass, and sulfide blebs by micro-x-ray absorption near-edge structure (μ-XANES) spectroscopy at beamline 13-IDE, Advanced Photon Source, Argonne National Laboratory. Spectra were collected in fluorescence mode from 2447 eV to 2547 eV, with a dwell time of two seconds on each point, using a Si [111] monochromator and a nominally focused beam, with effective diameter of <10x10 μm. Counts were recorded on a multi-element silicon drift detector x-ray spectrometer, equipped with two Si drift diode detectors. All analyses were done in a helium atmosphere, to avoid interaction between the incident photon beam and atmosphere. Incident beam intensity was set on the order 10^{10} photons per second, reflecting a balance between the intensity required to produce interpretable S-XANES spectra from materials with potentially low S-abundances (i.e., <1000 ppm) and the mounting evidence that very high photon density fluxes electronically damage Fe and S in silicate materials (e.g., Brounce et al. 2017; Cottrell et al. 2018). Each analysis was performed using a stationary beam.

We also collected elemental maps (Fig 1b, 2b, Supplemental Fig. 3, Supplemental Fig. 4) at the same beamline, using the same configuration, by recording fluorescence counts for 0.2 seconds per spot, over the specified 2-dimensional areas of interest (i.e., at each apatite grain) and recording fluorescence at 2475 eV (i.e., at the K-alpha absorption energy for S^{2-}) and at nearby elemental peaks for Na and P. Maps were generally collected over areas ~200 x 200 microns at 5 microns point spacing.

We also measured the sulfur abundances of apatites using a JEOL 8530 field emission electron microprobe at NASA's Johnson Space Center. An accelerating voltage of 15 kV, a nominal probe current of 20 nA, and a beam diameter of 3 μm were used during each analysis. Additionally, a ZAF correction was applied to all analyses using the Probe for EPMA software using procedures reported previously in McCubbin et al., (2010). Barite from SPI supplies was used as a primary standard, and the peak position for sulfide in apatite was checked on an internal troilite standard. In order to reduce or eliminate electron beam damage, we used a 5 μm defocused beam for standardization and 3 μm diameter beam for analysis of apatite grains in the Apollo samples. These differences in beam diameter between the standard and unknown have been shown to yield the same results within analytical error (McCubbin et al., 2011). These abundances are reported in Supplemental Table 1.

S-XANES spectra

The S-XANES spectra of lunar apatites reflect variable contributions of sulfate and sulfide, while sulfide blebs and mesostasis glass spectra show only sulfide-associated absorption features (Supplemental Fig. 1-4, Main text Fig 1-2). The S-XANES spectra of lunar apatites exhibit two to three main absorption features. The highest energy absorption feature is narrow and has varying intensity – sometimes altogether absent, and appears at ~2482 eV, coincident with S^{6+} absorption features from gypsum and other sulfate-bearing minerals (S Fig 1-2; Fleet 2005). The two lower energy, low intensity absorption features that are present in every spectra collected on apatite grains in Apollo thin sections – one narrow, appearing ~2470 eV and one broad, appearing ~2478 eV, are commonly attributed to the presence of S^{2-} (e.g., Fleet 2005), and match the shape of S-XANES spectra of troilite (Supplemental Fig. 1-2). The S-XANES spectra of sulfide blebs that appear in thin section near apatites have three absorption features –

two narrow and relatively low intensity features (~2466 eV, ~2470 eV) and one broad, relatively low intensity feature (~2478 eV; Supplemental Fig. 1). The absorption feature that appears ~2466 eV in sulfide blebs is critical, because that peak is entirely absent from any apatite spectra, demonstrating that the presence of S^{2-} in analyses of apatite, apparent from their S-XANES spectra, is not due to accidentally analyzing nearby sulfide blebs (Supplemental Fig. 1). Finally, the S-XANES spectra of mesostasis glass in sample 12039 contains two low intensity absorption features, one narrow (~2470 eV) and one broad (~2478 eV) that are attributed to the presence of S^{2-} and are similar in shape to that of troilite (Main text Fig 1). There is also sulfur present in the epoxies used to make the thin sections. The S-XANES spectra of these epoxies have two narrow absorption features at ~2482 eV and ~2474 eV. The epoxy used to make the thin section of sample 12309 that was used in this study (12039,4) contains less total sulfur than that of the epoxy used to make the thin section of sample 10044 that was used in this study (10044,33), apparent in the difference in signal-to-noise in their respective S-XANES spectra (Supplemental Fig. 1).

Calculating $S^{6+}/\Sigma S$ ratios

In order to quantify the relative contributions of sulfide and sulfate absorption features (i.e., to calculate $S^{6+}/\Sigma S$ ratios) and following the techniques described by Jugo et al. (2010) and Brounce et al. (2017), we first normalized all spectra so that the pre-edge region of the absorption spectra is at a value of zero and the post-edge region of the absorption spectra is at a value of one. Then, we used the S-XANES spectra of gypsum and troilite as endmember spectra, and fit each unknown using linear combinations of these endmember spectra. By assuming that the intensity of the absorption features for both S^{2-} and S^{6+} respond linearly to the concentrations of S^{2-} and S^{6+} in each analysis spot, we report $S^{6+}/\Sigma S$ ratios equal to the mixing proportions of the endmember spectra necessary to fit each unknown (e.g., Supplemental Fig. 2). Some apatites analyzed in this study have very low total sulfur concentrations, which results in decreased signal-to-noise ratio in S-XANES spectra, and thus diminishes our ability to confidently identify and fit the S^{6+} peak (~2482 eV) when it appears in low abundance. We thus estimate that the detection limit of S^{6+} in these S-XANES measurements in $S^{6+}/\Sigma S$ is ~0.03 (absolute). Our uncertainty in $S^{6+}/\Sigma S$, based on the reproducibility of fits from individual measurements, is +/- 0.01 (absolute). These calculated $S^{6+}/\Sigma S$ ratios are reported in Supplemental Table 1.

Thin section preparation

Standard thin sections 12309,4 and 10044,33 from the NASA Johnson Space Center Apollo collection were used in this study. Though specific records of the epoxy used in the preparation of 12309,4 and 10044,33 are not available, NASA Johnson Space Center curation described the preparation process for related thin section 12309,1 (i.e., a thin section taken from the same hand sample as 12309,4). To prepare thin section 12309,1, the exposed surfaces of each rock were impregnated with Epon 815 epoxy. A piece of the hand sample was then adhered to a glass slide using Araldite and polished with 3-micron diamond paste. The thin section surface was also exposed to alcohol, almag oil, and kerosene over the course of thin section preparation. It is not known specifically how these solvents and adhesives could interact with the lunar surface to produce secondary sulfate materials, but future work will test the possibility that oxidized sulfur signals originate from this process by testing thin sections prepared in various ways by NASA Johnson Space Center curation professionals.

APPENDIX FIGURES

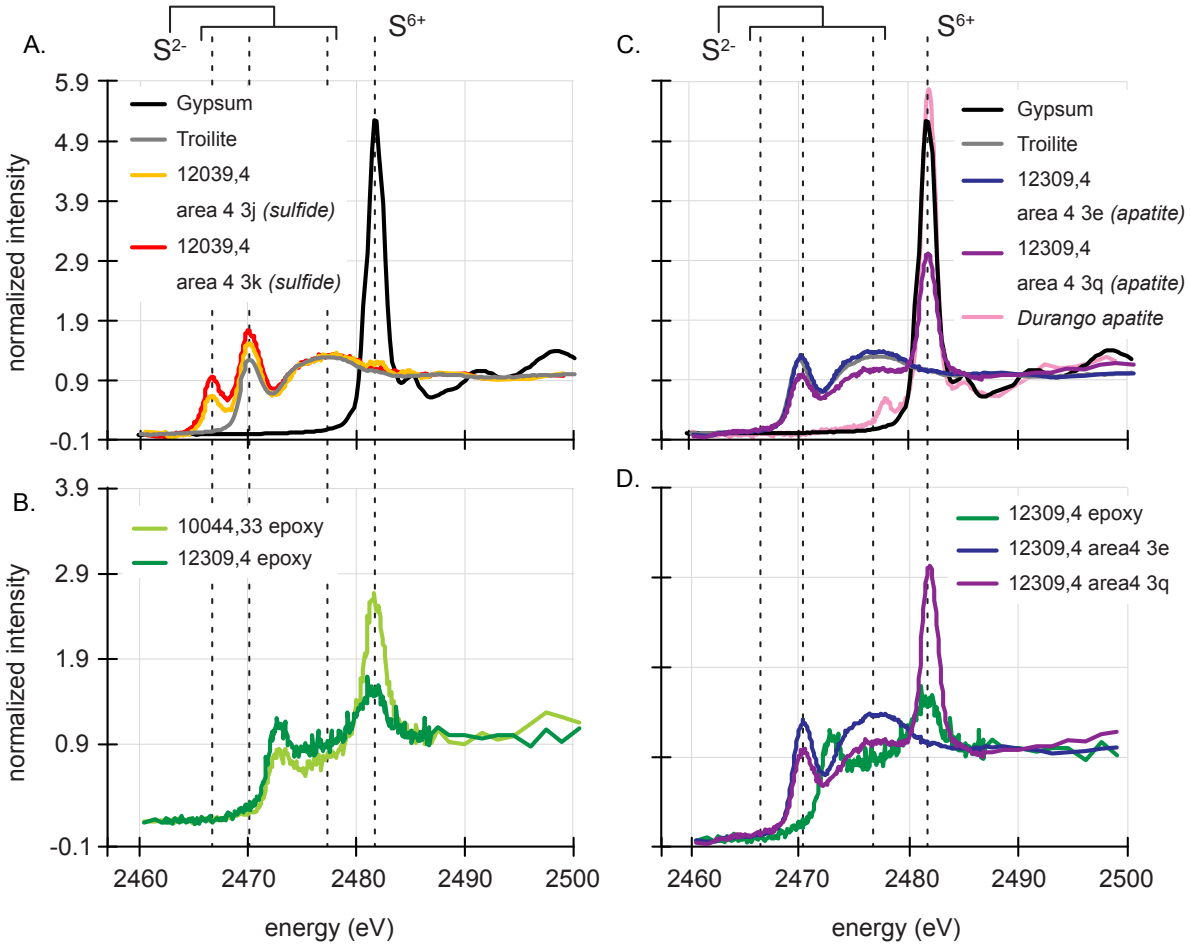

Supplemental Figure 1. Normalized S-XANES spectra for (**a**) gypsum (black curve), troilite (gray curve), and sulfide blebs in Apollo sample 12039,4 area 4 (red and yellow curve), (**b**) epoxy in thin section 10044,33 (light green curve) and 12039,4 (dark green curve), (**c**) apatite grains from 12039,4 that display a range in sulfide and sulfate absorption features (blue and purple curve), and a spectra on Durango apatite (pink curve), and (**d**) a comparison of the same spectra from apatite grains from 12039,4 in (**c**) compared to the epoxy spectra from the same thin section. The position of absorption peaks traditionally assigned to S^{2-} (2466, 2470, and 2478 eV) and S^{6+} (2482 eV) are marked in vertical gray lines.

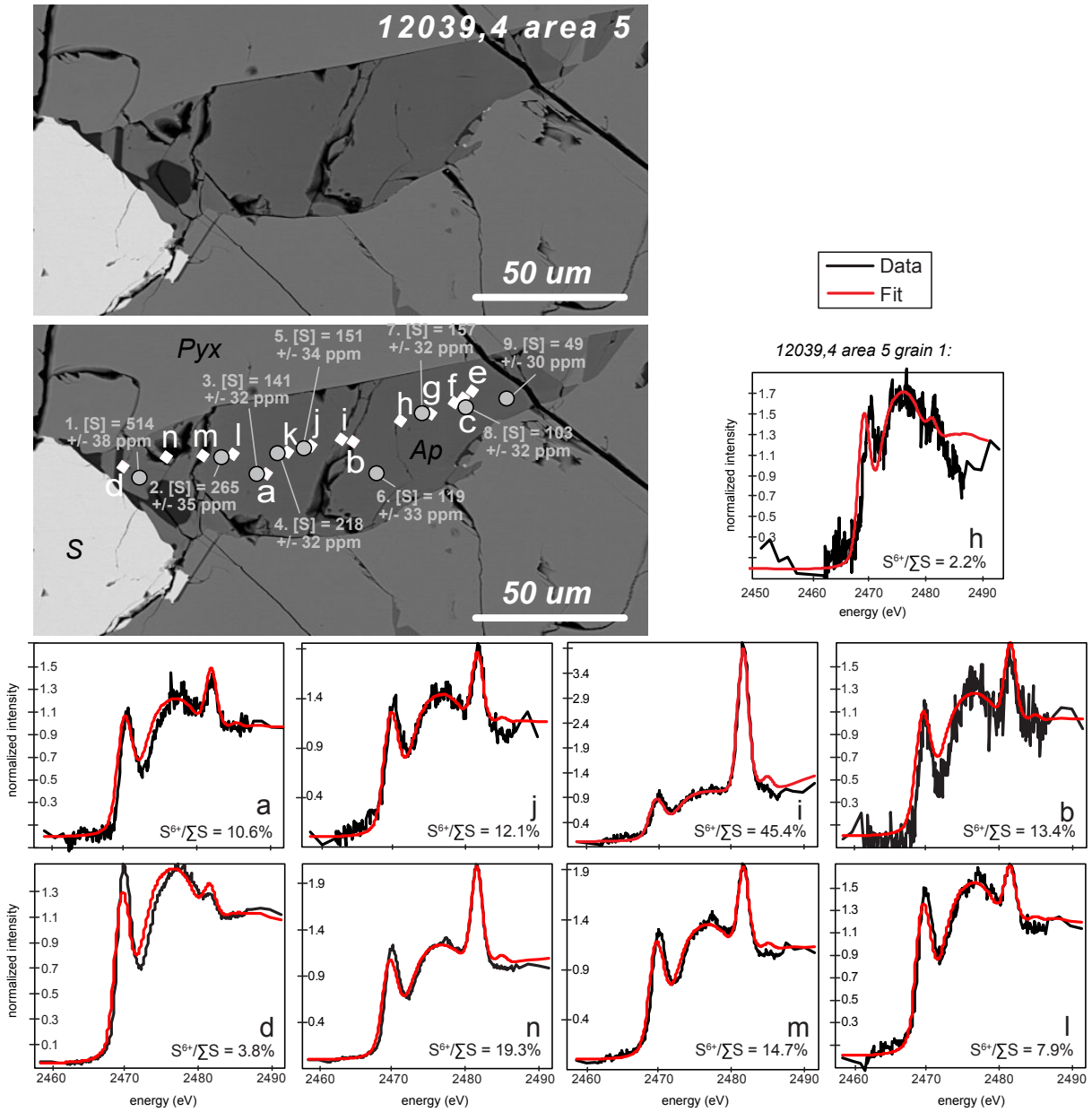

Supplemental Figure 2. Backscatter electron image that shows the locations of XANES (white diamonds) and EPMA (gray circles) analyses in thin section 12039,4 area 5. S-XANES spectra for selected analysis points on apatite. The black curve are data, the red curves are synthetic spectra produced from linear combinations of spectra collected on gypsum and troilite to provide a best fit to the data (see SI Appendix). Note that the signal-to-noise of each spectra decreases with increasing $S^{6+}/\Sigma S$, indicating that cracks and pits have more abundant sulfur that is specifically sulfate.

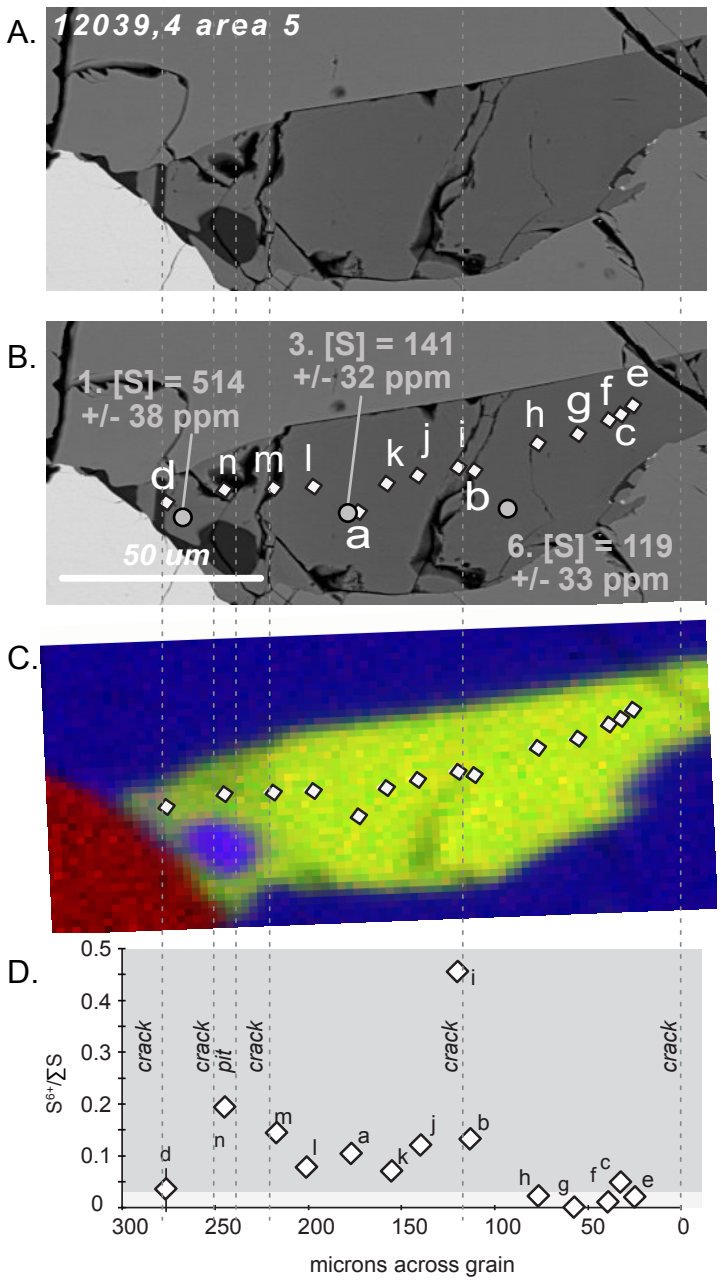

Supplemental Figure 3. (**a** and **b**) Backscatter electron and (**c**) S-P-Na (R-G-B) maps that shows the locations of XANES (white diamonds) and selected EPMA (gray circles) analyses in thin section 12039,4 area 5. Sulfide grains/blebs appear as red, apatite grains appear as green, and mesostasis glass appears as dark blue. (**d**) Calculated $S^{6+}/\Sigma S$ ratio from spectra at each analysis point from Fig. 1. Locations of cracks near analysis points are marked by gray dashed lines. Dark gray field marks $S^{6+}/\Sigma S > 3\%$. Analytical uncertainties are smaller than symbol size.

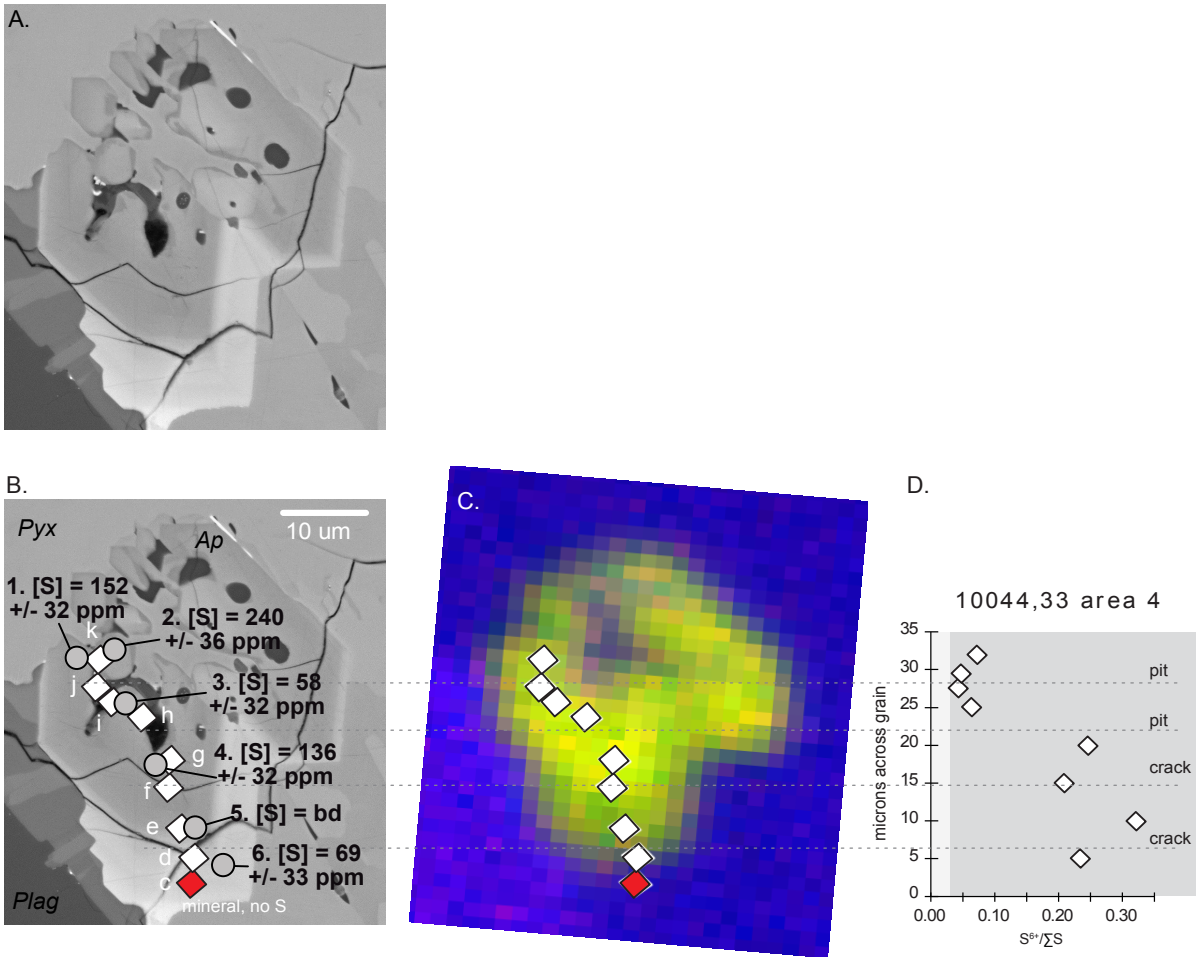

Supplemental Figure 4. (**a** and **b**) Backscatter electron and (**c**) S-P-Na (R-G-B) maps that shows the locations of XANES (white diamonds) and EPMA (gray circles) analyses in thin section 10044,33 area 4. Apatite grains appear as green. (**d**) Calculated $S^{6+}/\Sigma S$ ratio from spectra at each analysis point from Fig. 1. Locations of cracks near analysis points are marked by gray dashed lines. Dark gray field marks $S^{6+}/\Sigma S > 3\%$. Analytical uncertainties are smaller than symbol size.

Supplementary Figure 5

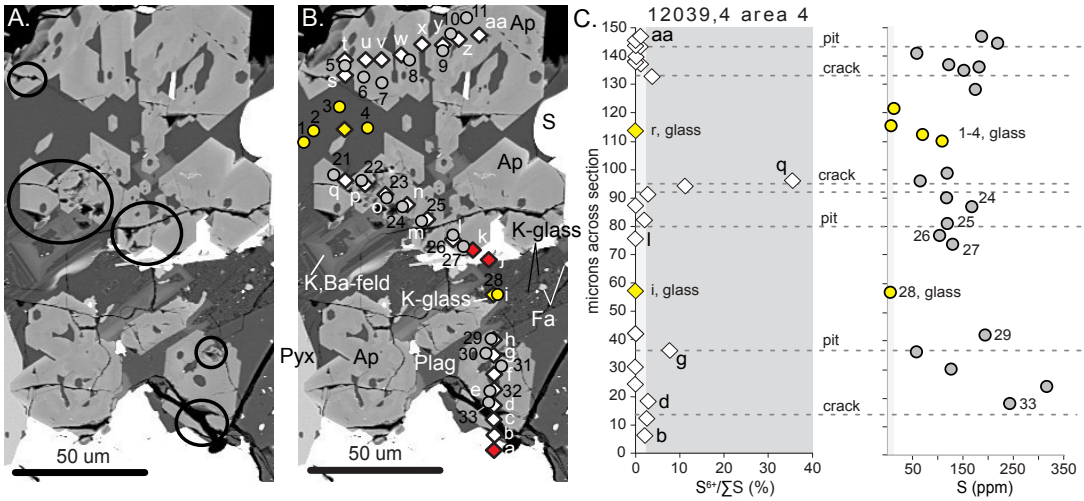

Supplemental Figure 5. (**a** and **b**) Backscatter electron images that show the locations of XANES (white diamonds) and EPMA (gray circles) analyses in thin section 12039,4 area 4. (**c**) Calculated $S^{6+}/\Sigma S$ ratio from spectra at each analysis point. Locations of cracks near analysis points are marked by gray dashed lines in (**c**) and (**d**), and circled in black in (**a**). Dark gray field marks $S^{6+}/\Sigma S > 3\%$. Analytical uncertainties are smaller than symbol size. (**d**) S concentrations determined via EPMA. Analytical uncertainties are listed in Supplementary Table 1.

Supplementary Figure 6

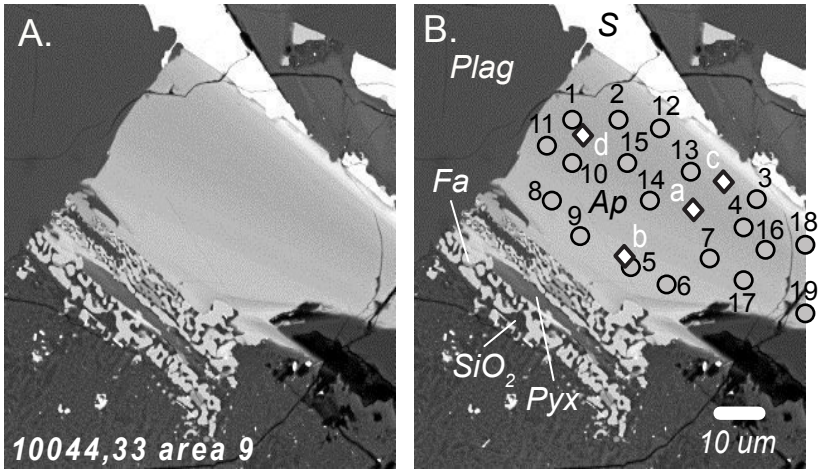

Supplemental Figure 6. (**a** and **b**) Backscatter electron images that show the locations of XANES (white diamonds) and EPMA (gray circles) analyses in thin section 10044,33 area 9. See Supplementary Table 1 for S concentrations and $S^{6+}/\Sigma S$.